Supporting Information

Direct Synthesis of Porous Organic Polymers with Protected Ethyne Monomer

Bo Chen,[a,b] Xinghua Guo,[a,b] Yongdong Jin,[c] Chuanqin Xia,* [c] Degao Wang* [a,b]

[a]Qianwan Institute of CNITECH, Zhongchuang 1st Road, Zhongchuang Park, Qianwan New Area, Ningbo, Zhejiang 315336, China.

[b]Ningbo Institute of Materials Technology and Engineering, Chinese Academy of Sciences (CAS), Ningbo, Zhejiang 315201, China.

[c]College of Chemistry, Sichuan University, Chengdu, Sichuan 610064, China.

Correspondance: xiachqin@163.com, wangdegao@nimte.ac.cn

Table of contents

1. Materials, instruments and methods

1.1 Materials

Bis(trimethylsilyl)acetylene (14630-40-1). 2,5-dimethyl-3-hexyne-2,5-diol (142-30-3), 1,4-bis(trimethylsilyl)-1,3-butadiyne (4526-07-2), 1,3,5-tribromobenzene (626-39-1), 2,4,6-tris(4-bromophenyl)-1,3,5-triazine (30363-03-2), 1,3,5-tris(4-bromophenyl)benzene (7511-49-1), tris(4-bromophenyl)amine (4316-58-9), 1,3,6,8-tetrabromopyrene (128-63-2), palladium(II) acetate (3375-31-3), tricyclohexylphosphine tetrafluoroborate (58656-04-5), pivalic acid (75-98-9), cesium carbonate (534-17-8), N,N-dimethylacetamide (127-19-5), pyrrole (109-97-7), propionic acid (79-09-4), 4-bromobenzaldehyde (1122-91-4), pyridine (110-86-1), bromobenzene (108-86-1), piperidine (110-89-4). All the above chemicals were purchased from commercial platforms with analytical purity and used without further purification.

Table S1. Monomers prices in this work and terminal alkynes in traditional Sonogashira polymerization.

Reaction	Monomers	CAS	Price
This method	bis(trimethylsilyl)acetylene	14630-40-1	152.0 ¥/25mL
This method	2,5-dimethyl-3-hexyne-2,5-diol	142-30-3	24.0 ¥/25g
This method	2,4,6-tris(4-bromophenyl)-1,3,5-triazine	30363-03-2	86.4 ¥/5g
This method	1,3,5-tris(4-bromophenyl)benzene	7511-49-1	78.4 ¥/5g
This method	tris(4-bromophenyl)amine	4316-58-9	25.6 ¥/5g
This method	1,3,6,8-tetrabromopyrene	128-63-2	82.4 ¥/5g
Traditional Sonogashira	1,3,5-triethynylbenzene	7567-63-7	2252.0 ¥/25g
Traditional Sonogashira	1,4-diethynylbenzene	935-14-8	2764.8 ¥/25g
Traditional Sonogashira	2,4,6-tris(4-ethynylphenyl)-1,3,5-triazine	425629-22-7	6684.6 ¥/25g
Traditional Sonogashira	1,3,5-tris(4-ethynylphenyl)benzene	71866-86-9	3256.0 ¥/25g

The prices were obtained from https://www.tansoole.com/ on Jan. 26th 2026.

1.2 Instrumments

^{1}H and **^{13}C NMR**. The NMR experiments were carried out on a 400 MHz Bruker AVANCE III HD spectrometer.

Fourier transform infrared (**FT-IR**). IR spectra were measured on a Bruker INVENIO R infrared spectrometer with the range between 4000 to 400 cm^{-1} using reflection mode. Pure KBr disc was used to record background, and the sample discs were tested as soon as they were prepared to prevent from oxidation or moisture.

Organic elemental analysis (C, H, N, S). Elemental analysis was performed on a CARLO ERBA 1106.

Powder X-ray diffraction (PXRD). Data were collected on a Panalytical EMPYREAN diffractometer using Cu Kα radiation with 2 theta range of 2° to 45°.

Nitrogen sorption analysis. surface areas were measured according to nitrogen adsorption and desorption at 77 K on a Quantachrome Autosorb-iQ. The samples were degassed at 100°C for 12 h under high vacuum before analysis.

Scanning electron microscopy (SEM). SEM images and energy-dispersive X-ray spectroscopy (EDX) were carried out on a JEOLA JSM-7500F.

Thermogravimetric analysis (TGA). The TGA curve was recorded on a Shimadzu DTG-60(H) with the temperature range from 30 to 800°C at a rate of 10°C/min under nitrogen.

UV−Vis diffuse reflectance spectra (UV−vis DRS). The UV-Vis spectrum was recorded on a Shimadzu UV-3600.

High resolution transmission microscopy (TEM). SEM images and EDX analysis were carried on a FEI Talos F200S.

Raman. Raman spectrum was recorded on laser confocal micro-raman spectrometer (LAbRAMHR Evolution) from HARIBA.

Inductively coupled plasma optical emission spectrometer (ICP-OES). The concentration of Pd was tested by Ultima Expert ICP optical emission spectrometer from HARIBA. 20 mg of pTBT-En was digested by concentrated HNO_3 and H_2O_2 under reflux for 2 days. The solution was filtered and diluted to 50 mL. Then, the concentration of Pd was tested. The Pd content was calculated with the following formula.

$$Pd\ content\ (\%) = \frac{c(mg/L) \times 0.05\ (L)}{20(mg)} \times 100\%$$

1.2 Methods

In Electrochemical analysis, fluorine-doped conductive glass was used as the working electrode, a platinum sheet electrode as the counter electrode, and an Ag-AgCl electrode as the reference electrode. A 0.2 mol/L Na_2SO_4 solution was used as electrolyte. The POPs sample was mixed with 5% Nafion (perfluorosulfonic acid resin) in ethonal, and then dropped onto a 1×1 cm^2 area of fluorine-doped tin oxide (FTO) glass, and then the conductive glass was transferred to an oven for drying at 65°C for 5 hours before use.

Mott-Schottky analysis. In the Mott-Schottky test, the test range was from −1.4 V to 0.10 V, with 300, 500, and 700 Hz as modulation frequencies, and. The obtained flat band potential could be converted to the value corresponding to the saturated calomel electrode via $E_{SCE} = E_{Ag\text{-}AgCl} + 0.04$ V.

Photocurrent. The photocurrent of the CMPs was performed under irradiation 300 W Xe lamp. The light source was manually blocked every 20 seconds interval to collect the changes in photocurrent signals.

Electrochemical impedance (EIS). The EIS spectrum of POPs was recoded from 100000 Hz high frequency to 0.01 Hz low frequency. The results were converted to Nyquist Plot Z''-Z' form.

2. Synthetic procedures

2.1 CsOPiv

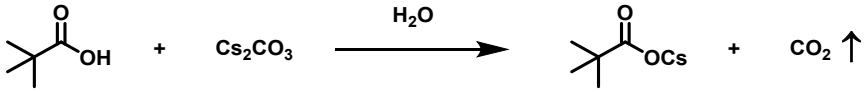

Scheme S1. The synthetic route for CsOPiv[1].

As depicted in the synthetic method shown above, 3.164 g (31 mmol) of pivalic acid and 5.000 g (15.3 mmol) of cesium carbonate were weighed into a small beaker, followed by the addition of 3 mL of water. Upon stirring, a large number of bubbles were generated. After the bubbling ceased, the mixture was heated to 50 °C and stirring was continued for 10 minutes. Subsequently, the mixture was transferred to a vacuum drying oven, where the temperature and vacuum degree were gradually increased for drying. Finally, complete drying was achieved at 100 °C with the assistance of phosphorus pentoxide. Due to the high hygroscopicity of cesium pivalate, the prepared product was stored in a glove box.

2.2 TBP-Br_4

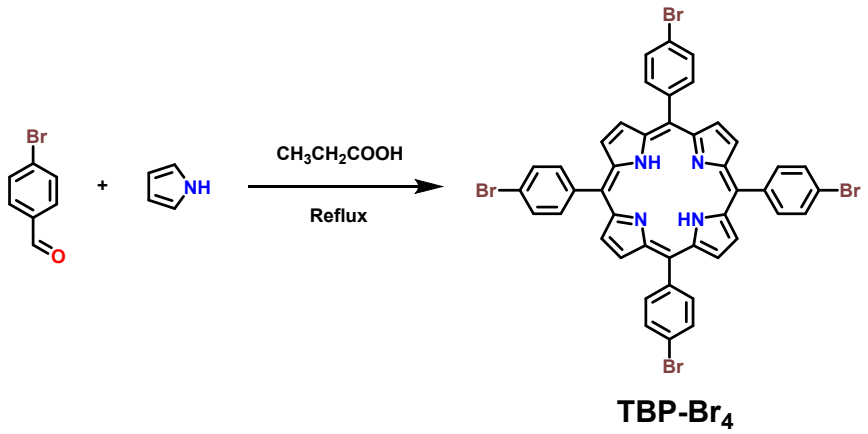

Scheme S2. The synthetic route for TBP-Br_4[2].

The synthesis method of 5,10,15,20-tetrakis(4-bromophenyl)porphyrin, namely TBP-Br_4, is as shown in the above figure. 18.5 g (100 mmol) of 4-bromobenzaldehyde was weighed and dissolved in 380 mL of propionic acid, and heated to reflux (boiling point of propionic acid: 141°C). 6.7 g

(100 mmol) of pyrrole was weighed and slowly added dropwise into the boiling propionic acid. After the addtion was completed, stirring and refluxing were continued for 2 hours. The mixture was cooled to room temperature and filtered, and the filter cake was washed with water and methanol to obtain a blue crude product. Subsequently, recrystallization was performed using pyridine to obtain 5.26 g of a solid with a yield of 21%. ^{1}H NMR ($CDCl_3$) δ = 8.84 (s, 8H), 8.05 (d, 8H), 7.91 (d, 8H), −2.87 (s, 2H).

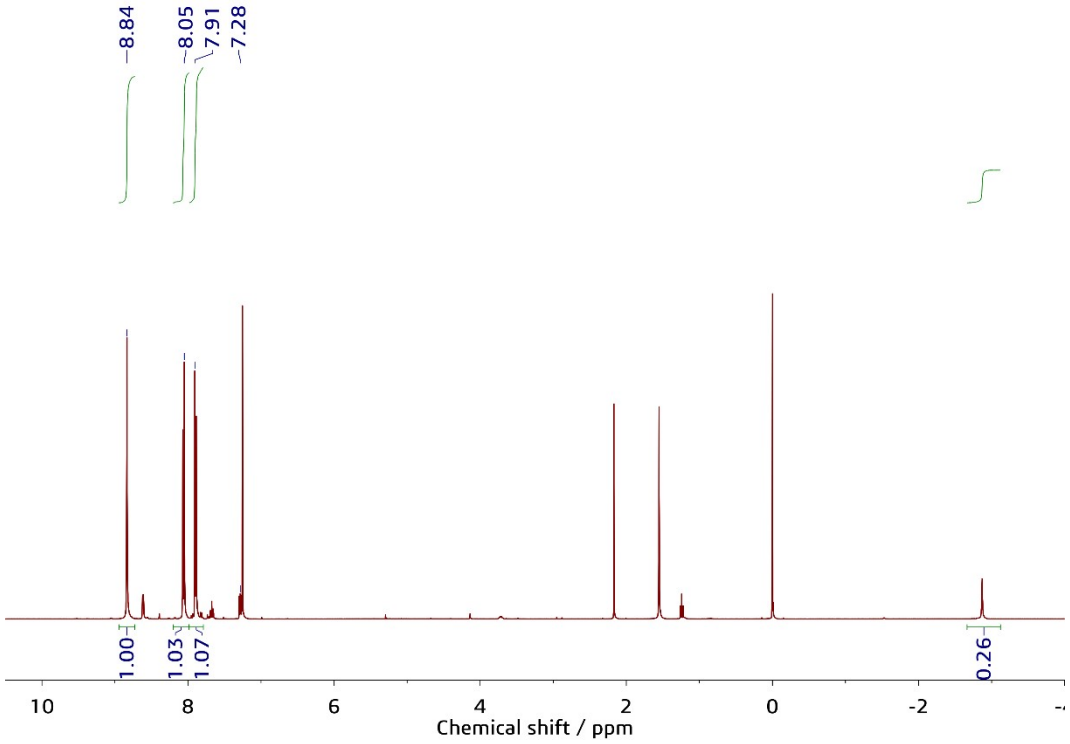

Figure S1. The ^{1}H NMR spectrum of TBP-Br_4 in $CDCl_3$.

2.3 Model reaction

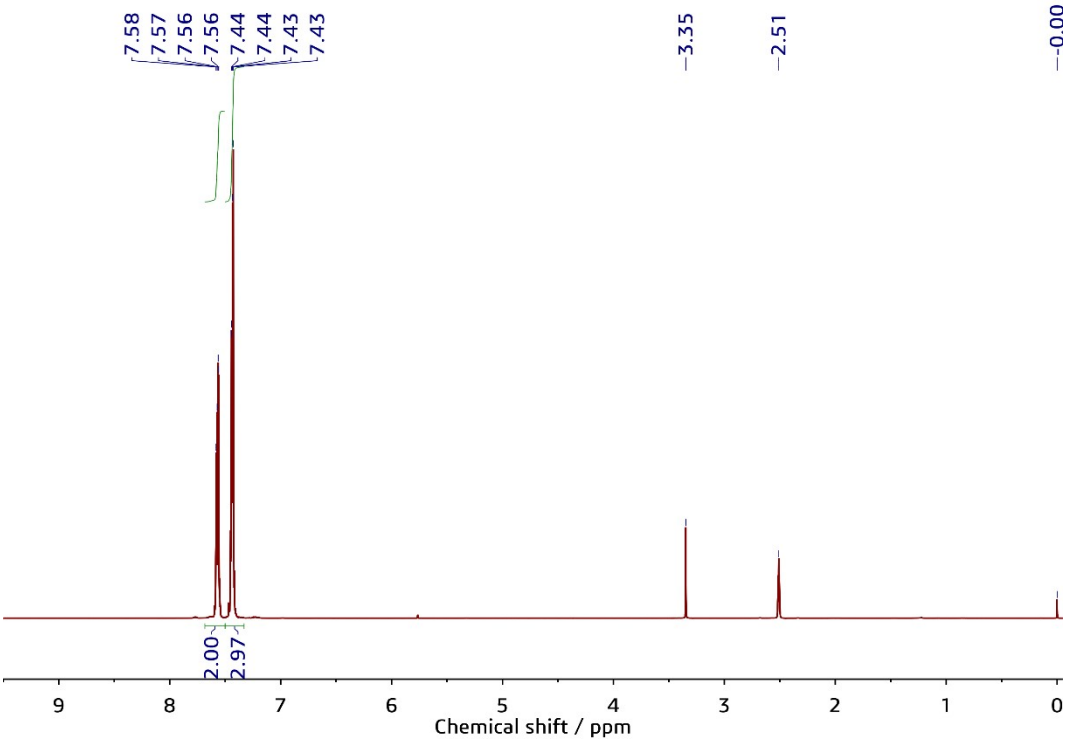

Figure S2. The ^{1}H NMR spectrum of product of model reaction in DMSO-d6.

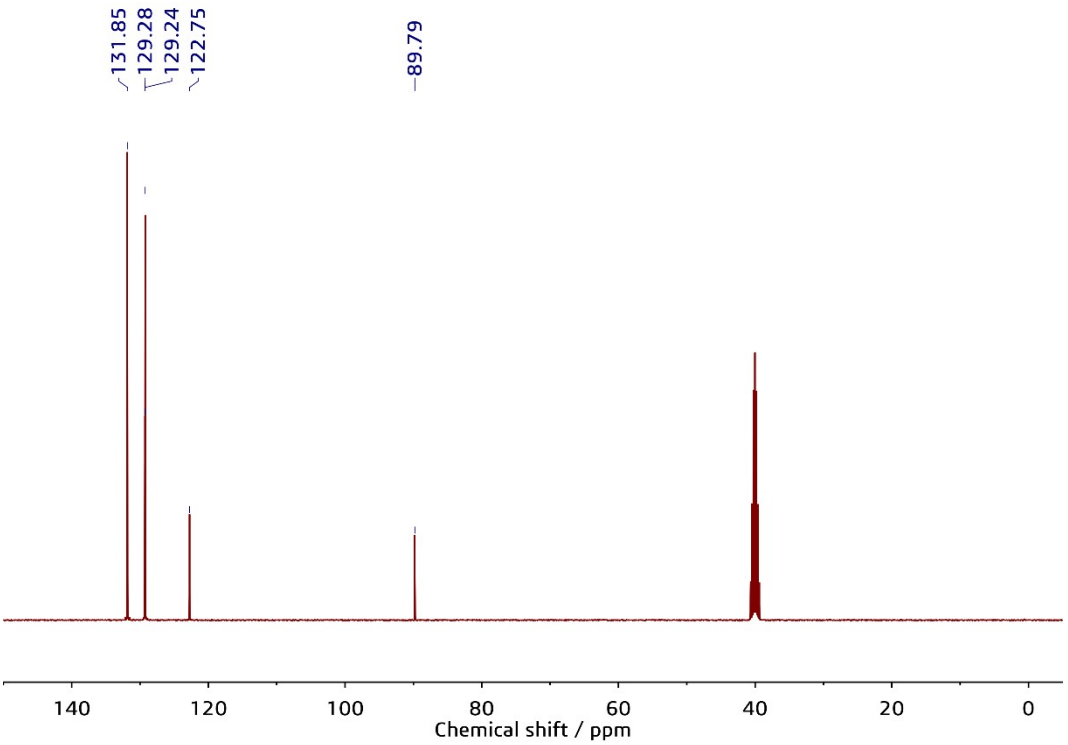

Figure S3. The ^{13}C NMR spectrum of product of model reaction in DMSO-d6.

2.4 POPs

2.4.1 Catalyst optimization

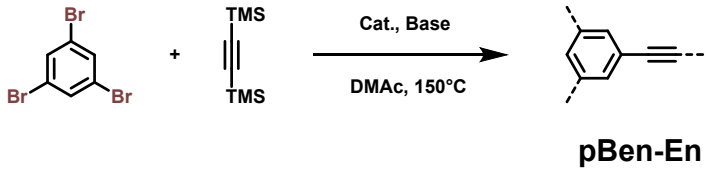

Scheme S3. The synthetic route for pBen-En

Table S2. Screening results of catalytic conditions.

Entry	Cat.	Base	Yield
1	$Pd(OAc)_2$ + $PCy_3{\cdot}HBF_4$	CsOPiv	117%
2	$Pd(PPh_3)_2Cl_2$	CsOPiv	oligomer
3	$Pd(dppf)Cl_2$	CsOPiv	196%
4	$Pd(PPh_3)_4$	CsOPiv	161%
5	$Pd(OAc)_2$ + $PCy_3{\cdot}HBF_4$	DBU	171%
6	$Pd(OAc)_2$ + $PCy_3{\cdot}HBF_4$	Cs_2CO_3	123%

Oligomer refers to the resulting polymer that is present in small quantities and soluble in some organic solvents used during the washing process. Conditions: 1,3,5-tribromobenzene 0.30 mmol; En-TMS_2 0.45 mmol; catalyst 0.02 mmol; base 1.8 mmol; DMAc 6 mL; under Ar gas protection; reaction temperature 150 °C; reaction time 48 h. The over high yield exceeding 100% is mainly attributed to unreacted Br and TMS groups.

2.4.2 Monomer concentration optimization

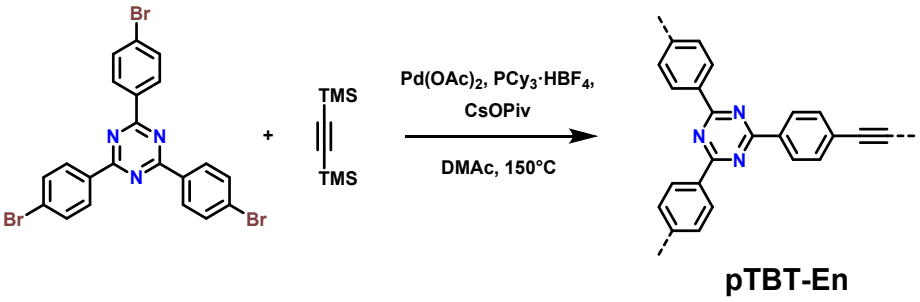

Scheme S4. The synthetic route for pTBT-En

Table S3. Screening results of monomer concentration.

Entry	Monomer concentration	Yield
1	0.1 mol/L	97%
2	0.05 mol/L	96%
3	0.033 mol/L	93%

Conditions: TBT-Br_3 0.30 mmol; En-TMS_2 0.45 mmol; catalyst $Pd(OAc)_2$ + PCy_3·HBF_4, 0.02 mmol + 0.04 mmol; base CsOPiv 1.8 mmol; under Ar gas protection; reaction temperature 150 °C; reaction time 48 h.

The monomer concentrations (TBT-Br_3/DMAc, mol/L) were controlled by different DMAc volume. 3, 6 and 9 mL DMAc were added in Entry 1, 2 and 3, respectively. All 3 entries had similar yields between 93%~97%. However, in entry 1 and 2, the solvent was too little, and induced uneven stirring, which should be avoided in POPs synthesis.[3]

2.4.3 POPs synthesis with acetone protected ethyne

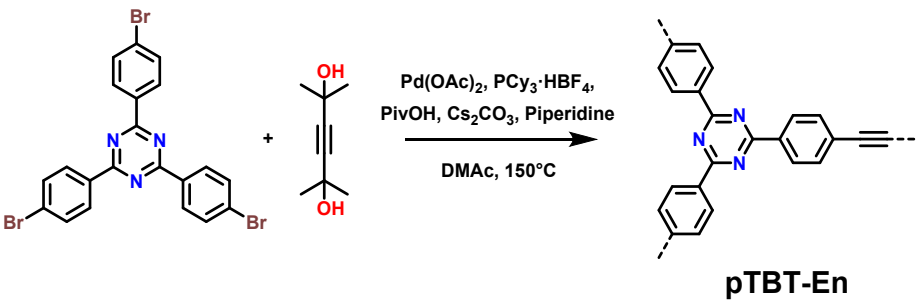

Scheme S5. The synthetic route for pTBT-En using acetone protected ethyne

For acetone protected ethyne (En-HME$_2$), Cs_2CO_3 (2.0 mmol), PivOH (0.2mmol) and piperidine (0.1 mmol) were used as base. Piperidine was added to increase the reaction conversion degree. All other conditions were the same as Entry 3 in 2.4.2. The yield was 109%.

2.4.4 POPs synthesis with TMS protected 1,3-butadiyne

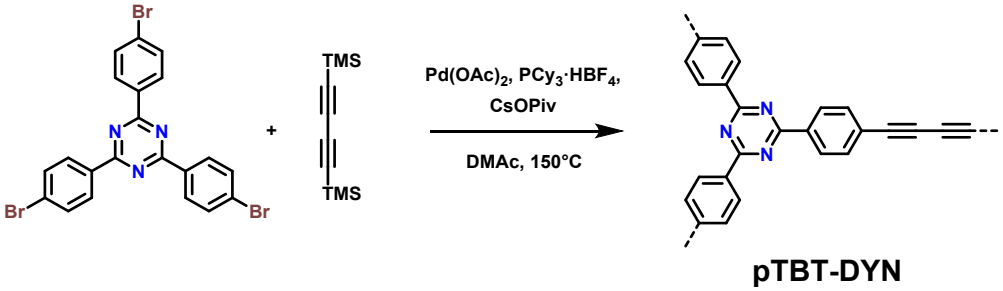

Scheme S6. The synthetic route for diyne-linked POPs of pTBT-DYN

To obtain diyne-linked POPs, TMS protected 1,3-butadiyne (0.45 mmol) was used as monomer. All other conditions were the same as Entry 3 in 2.4.2. However, when the reaction system began to heat up, a black sold formed rapidly. The same black solid was also observed without addition of TBT-Br$_3$, which indicated that TMS protected 1,3-butadiyne is not stable under such condition. For further attempts to get diyne-linked POPs, lower reaction temperature and stronger base could be taken into consideration.

3 Characterization of POPs

Table S4. Organic elemental analysis and EDX elemental analysis result.

POPs	Content (%)	C	N	H	Br	Si	Pd
pTBT-En	calculated	84.19	12.27	3.53	-	-	-
	organic EA	73.33	10.58	4.53	-	-	-
	EDX EA	73.26	17.69	-	6.92	0.12	2.01
pTBB-En	calculated	95.55	0	4.45	-	-	-
	organic EA	85.70	-	5.15	-	-	-
	EDX EA	92.34	-	-	4.85	0.25	2.56
pTBA-En	calculated	90.62	5.03	4.35	-	-	-
	organic EA	82.17	5.03	5.21	-	-	-
	EDX EA	81.06	11.55	-	4.13	0.19	3.06
pTBP-En	calculated	87.52	8.51	3.98	-	-	-
	organic EA	76.50	7.70	4.18	-	-	-
	EDX EA	75.18	11.55	-	11.99	0.15	1.12
pPYR-En	calculated	97.54	0	2.46	-	-	-
	organic EA	79.81	-	3.79	-	-	-
	EDX EA	90.60	-	-	7.27	1.77	0.22

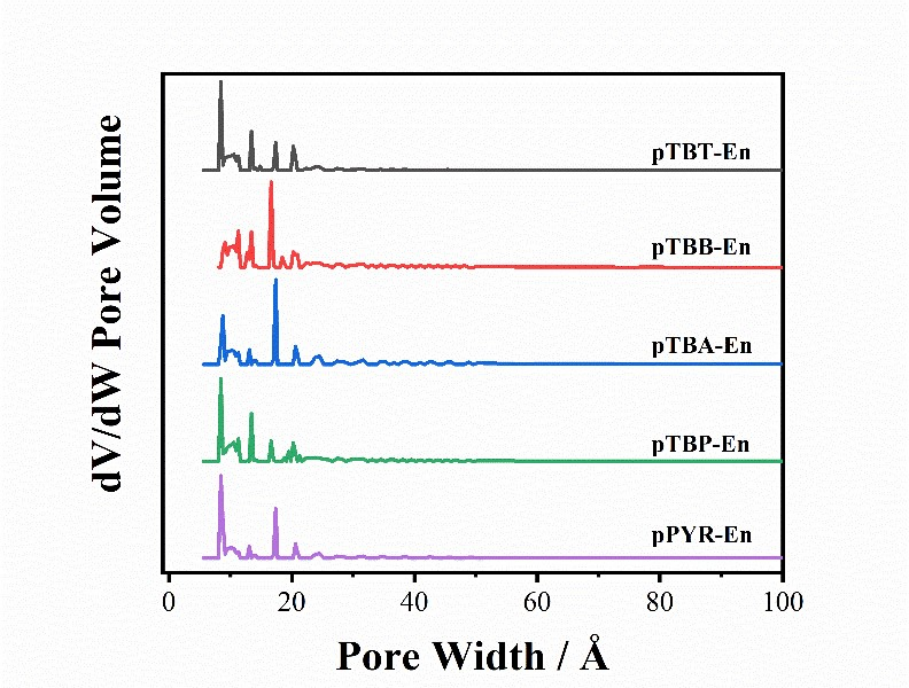

Figure S4. Pore size distribution of 5 POPs.

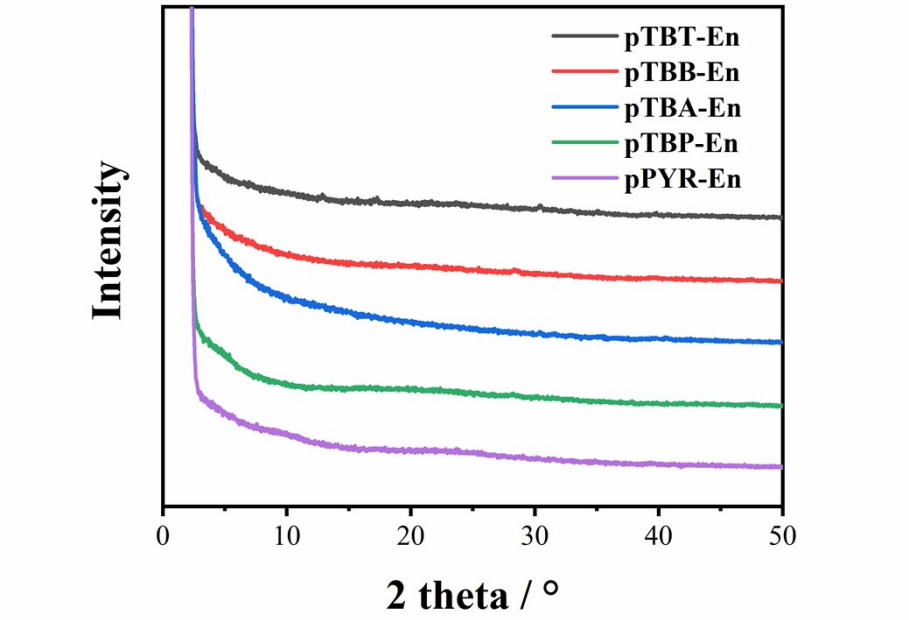

Figure S5. Powder XRD patterns of 5 POPs.

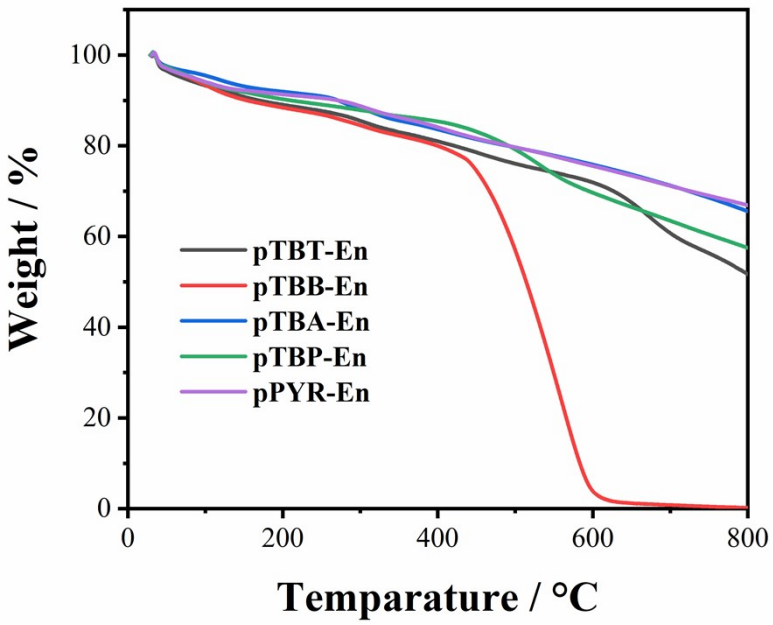

Figure S6. TGA curves of 5 POPs.

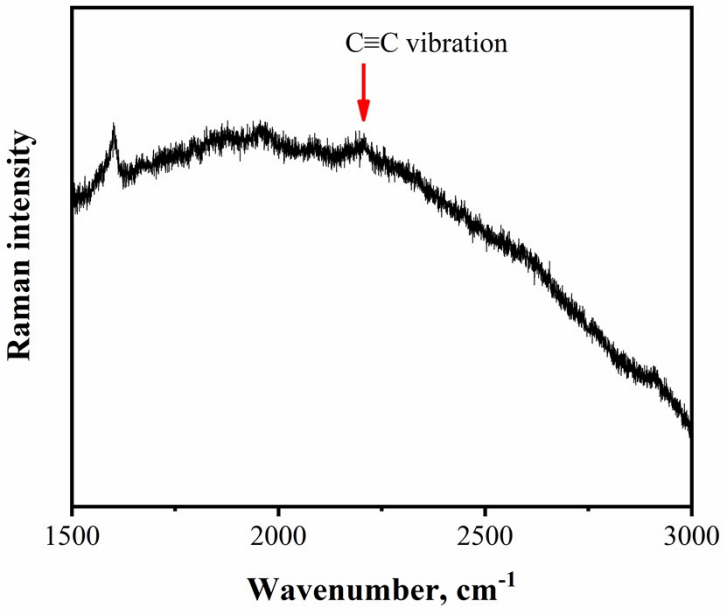

Figure S7. Raman spectrum of pTBT-En.

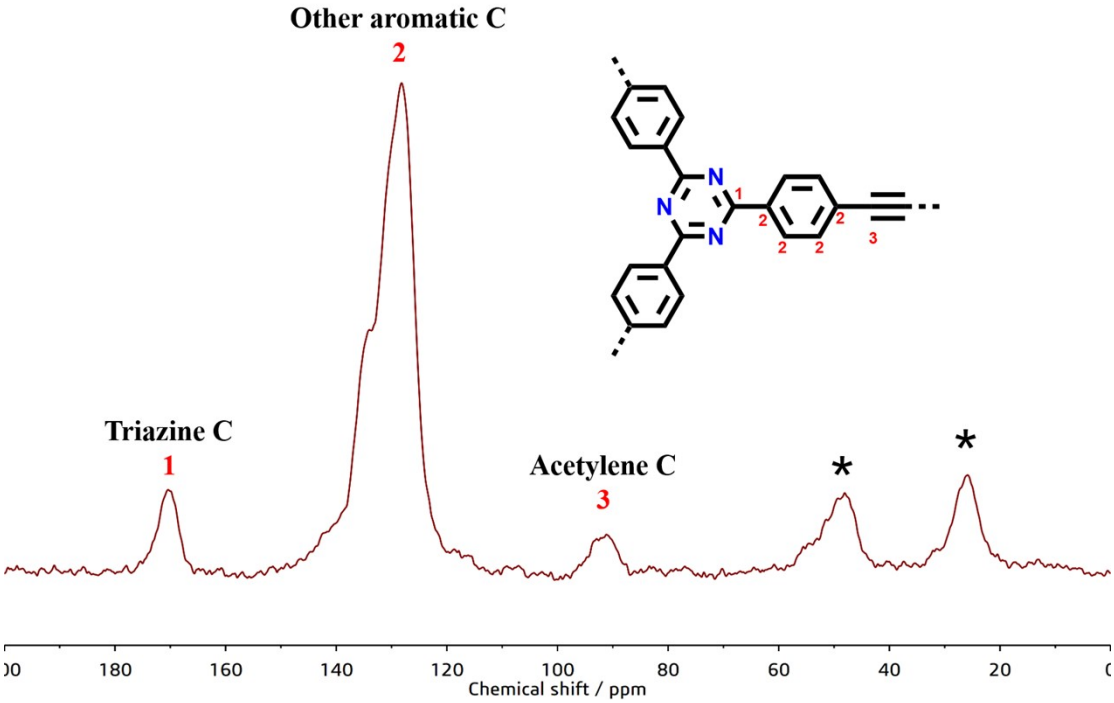

Figure S8. Solid state ^{13}C NMR spectrum of pTBT-En, satellite peaks are signed with asterisks (*).

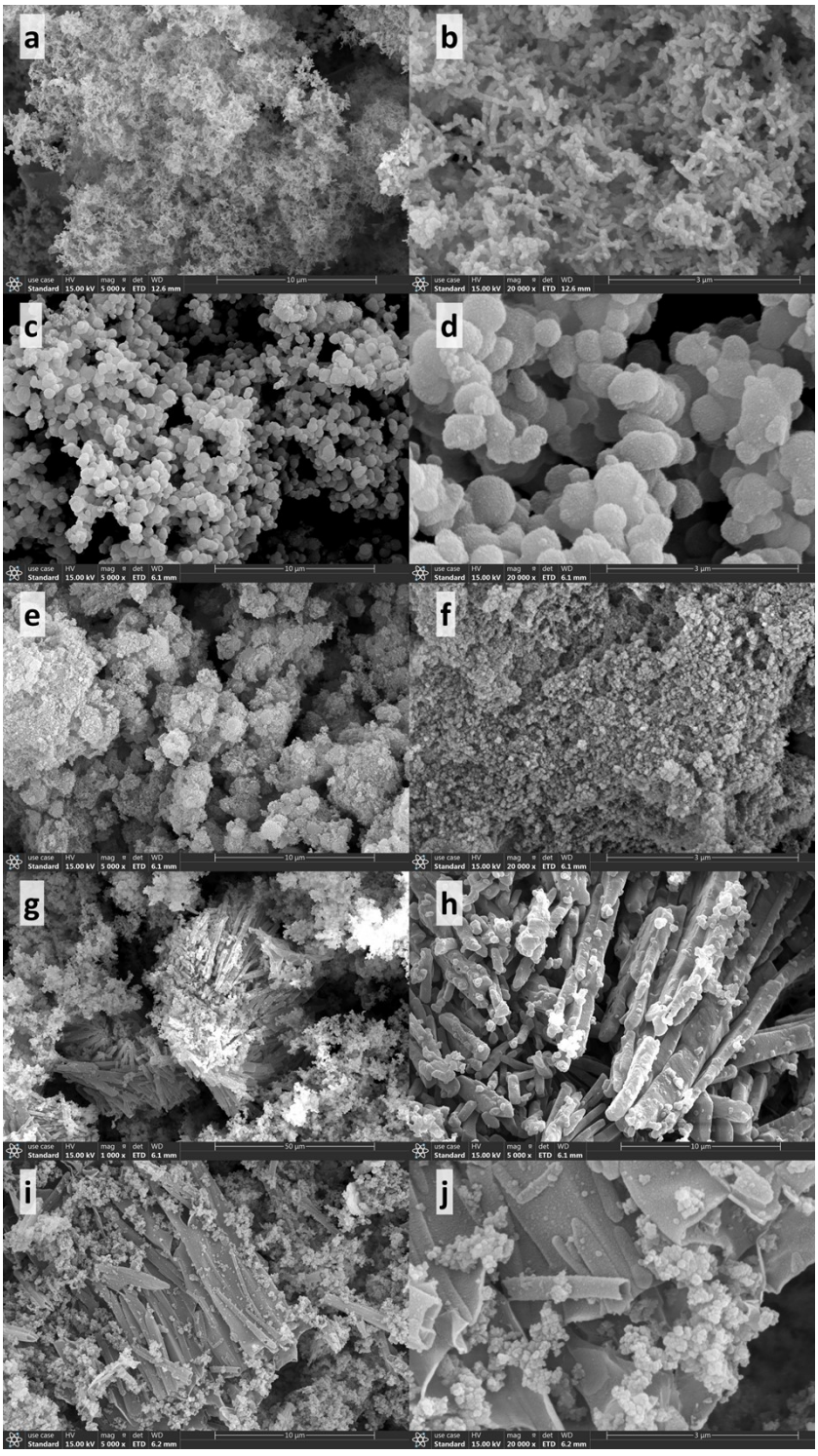

Figure S9. SEM images of 5 POPs.

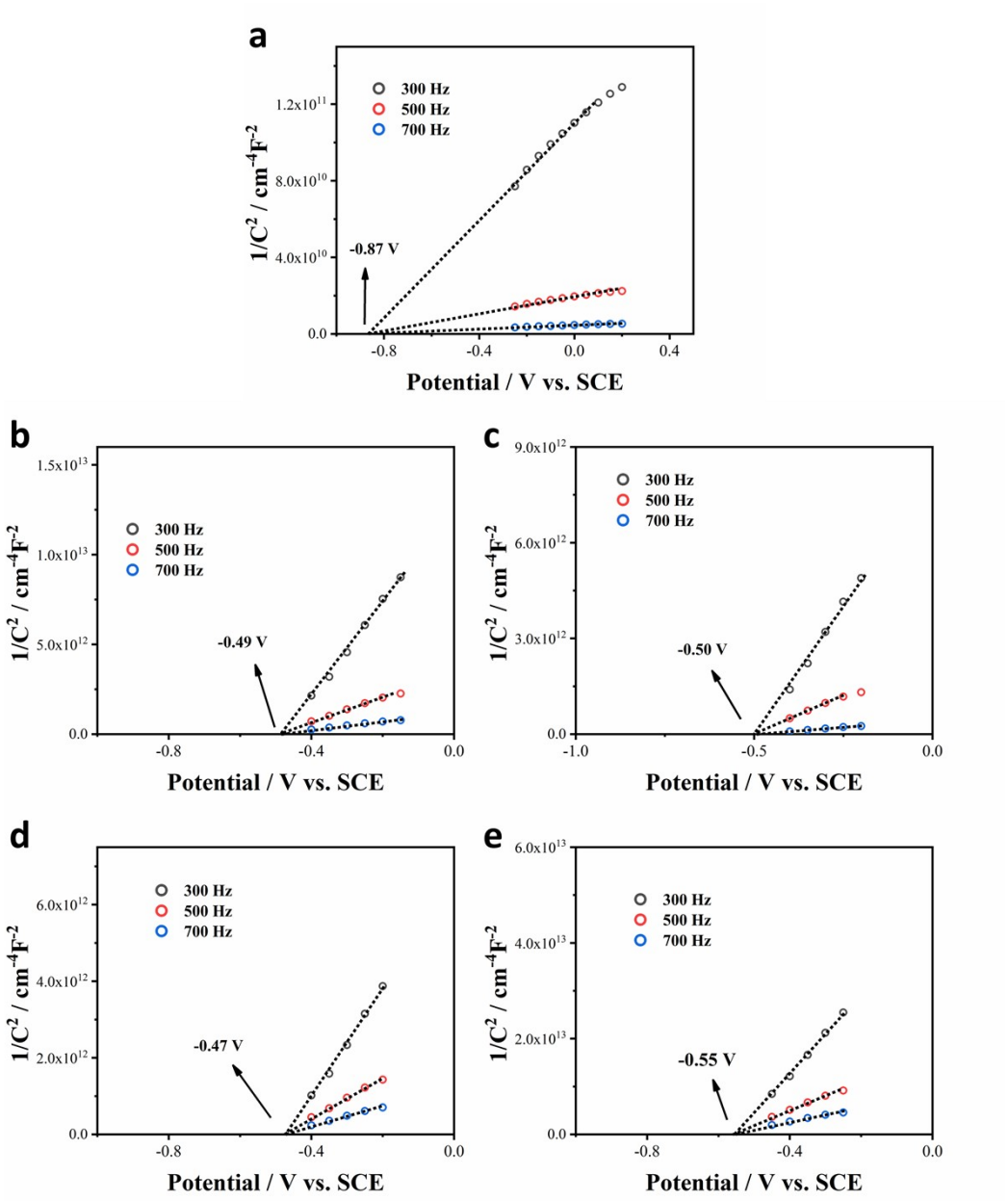

Figure S10. Mott-Schottky results and corresponding flat bands of 5 POPs. pTBT-En (a), pTBB-En (b), pTBA-En (c), pTBP-En (d) and pPYR- En (e).

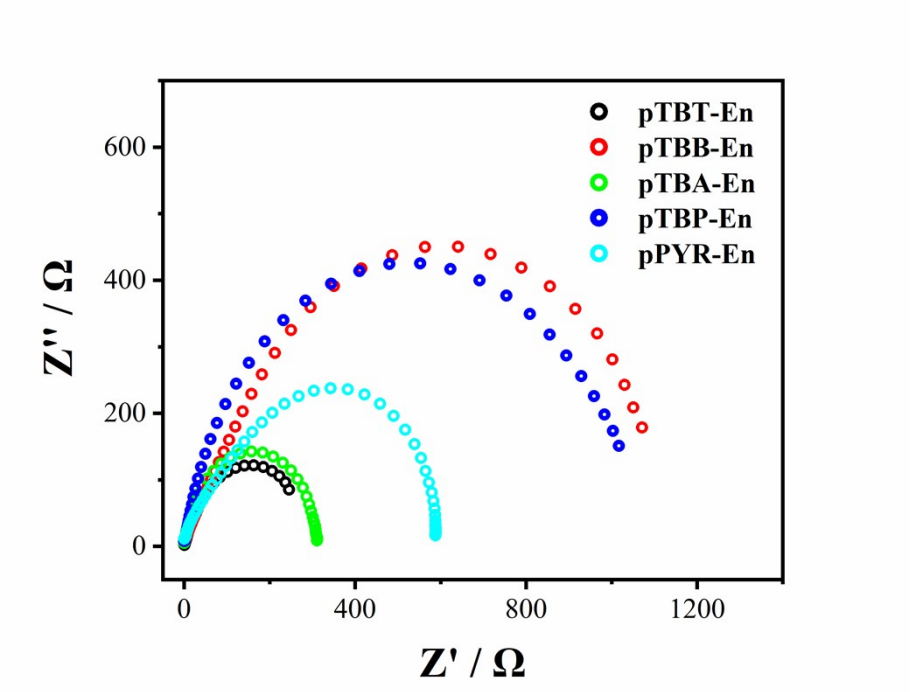

Figure S11. Nyquist plots of 5 POPs.

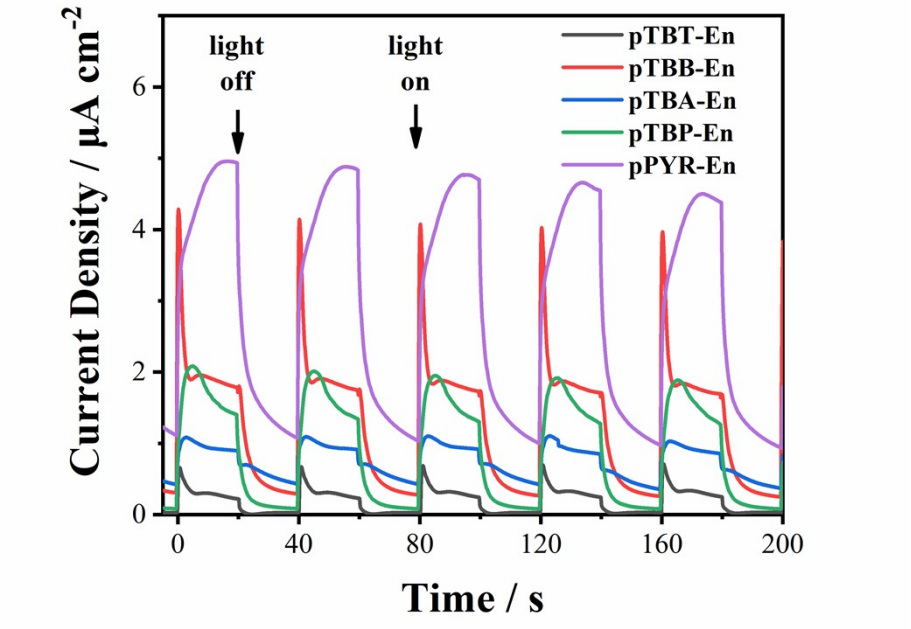

Figure S12. Photocurrent response intensity of 5 POPs.

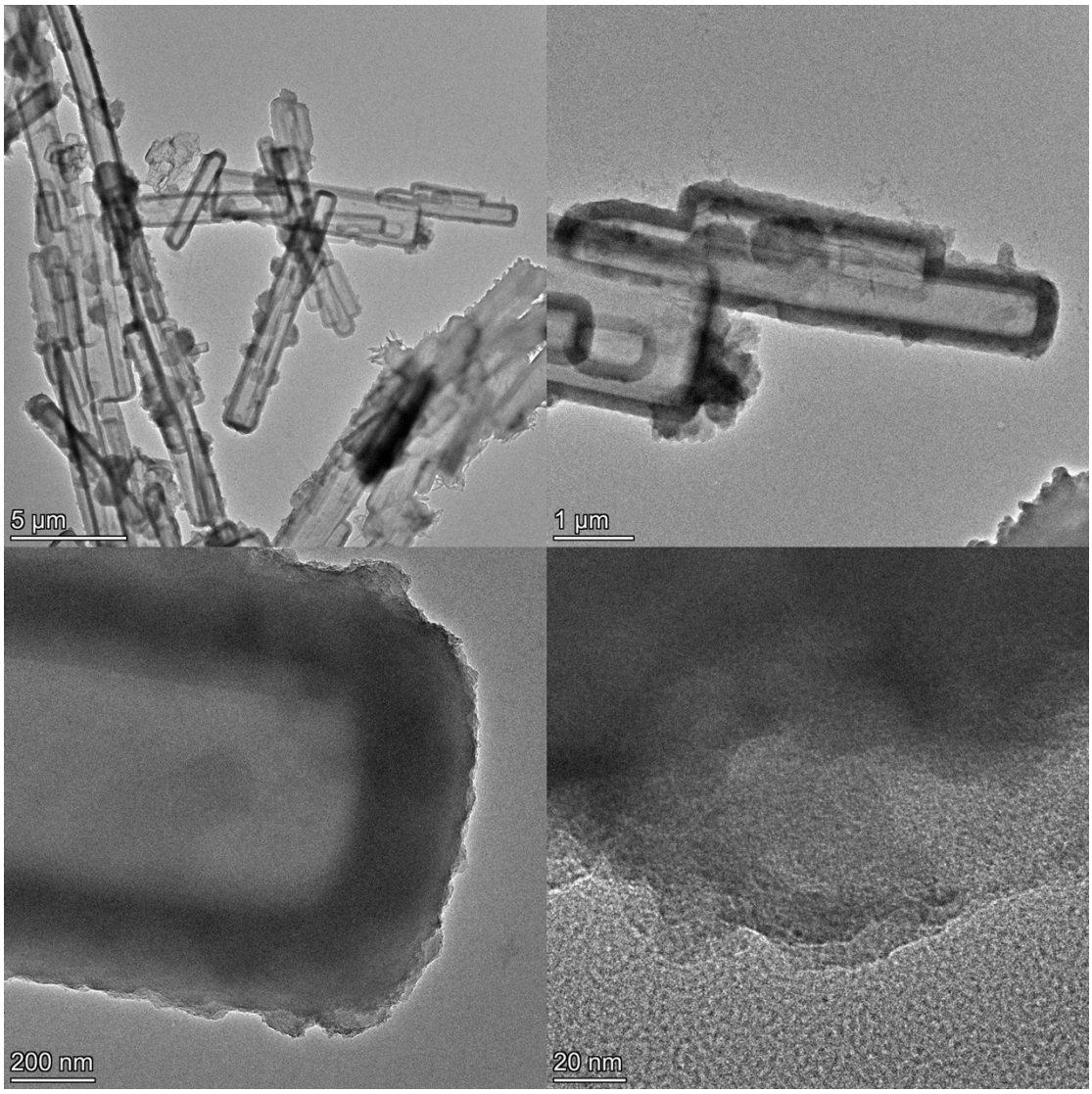

Figure S13. High resolution TEM images of pTBT-En.

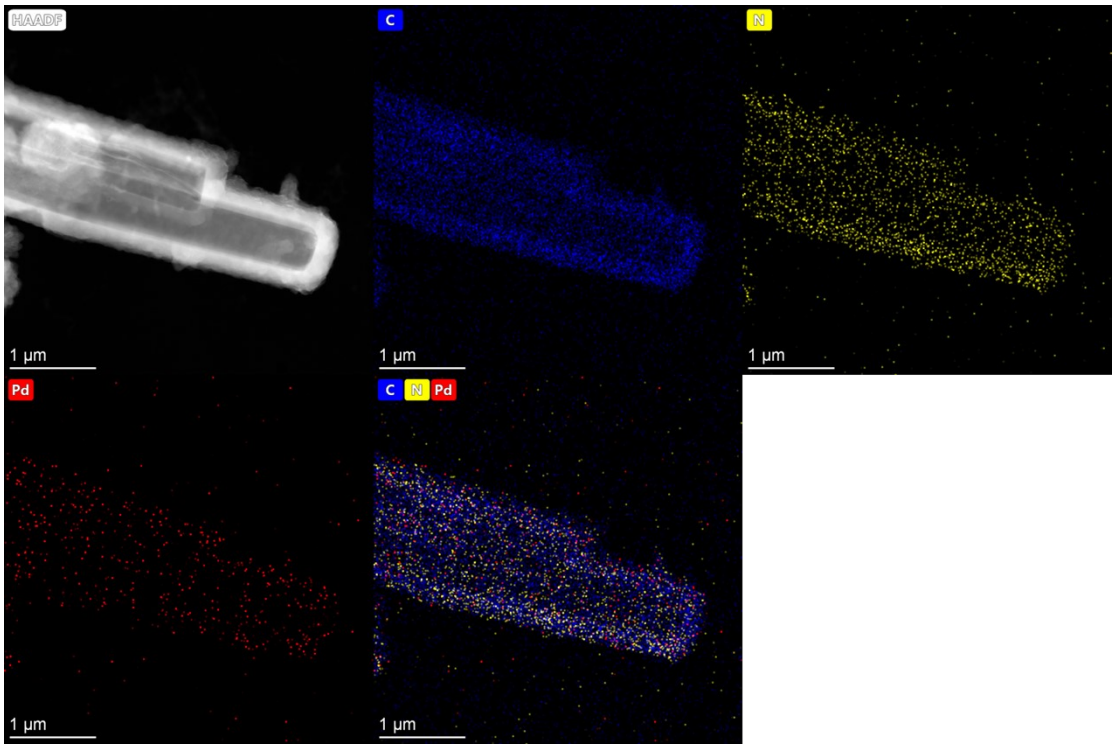

Figure S14. TEM EDX elemental mapping of C, N and Pd of TBT-En.

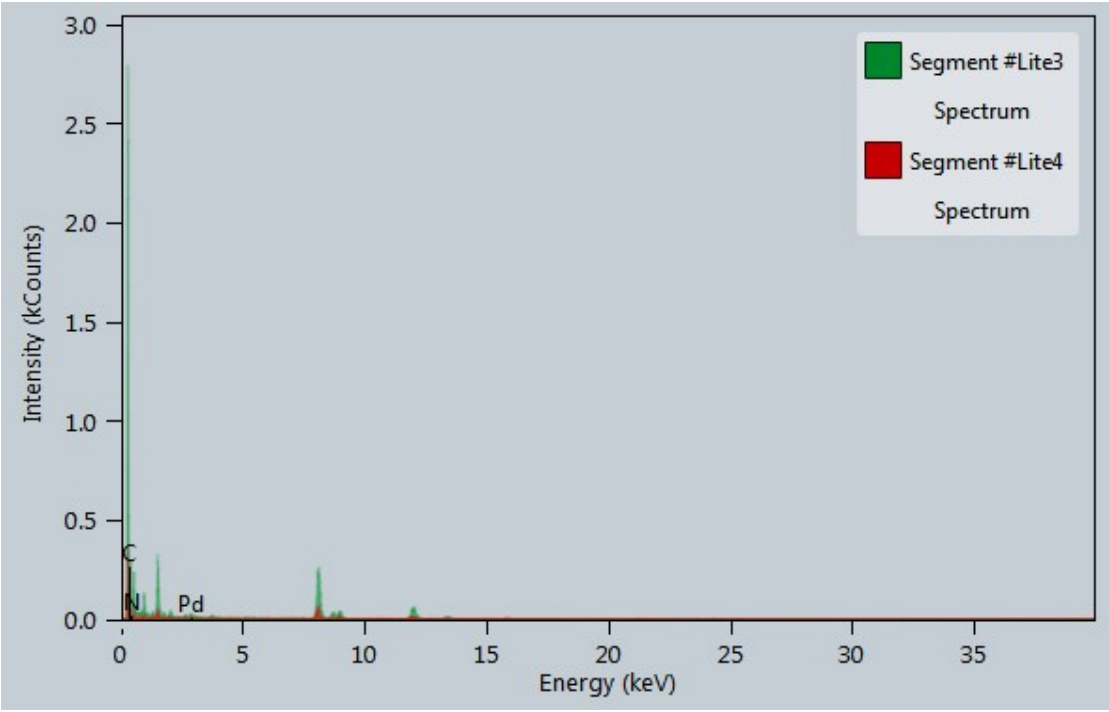

Figure S15. TEM EDX elemental analysis of pTBT-En.

Table S5. TEM EDX elemental analysis result of pTBT-En.

Z	Element	Family	Atomic Fraction (%)	Atomic Error (%)	Mass Fraction (%)	Mass Error (%)	Fit error (%)
6	C	K	94.74	7.46	91.53	5.13	4.04
7	N	K	4.92	1.05	5.55	1.14	2.68
46	Pd	L	0.34	0.05	2.92	0.36	1.51

4 Photocatalytic performance

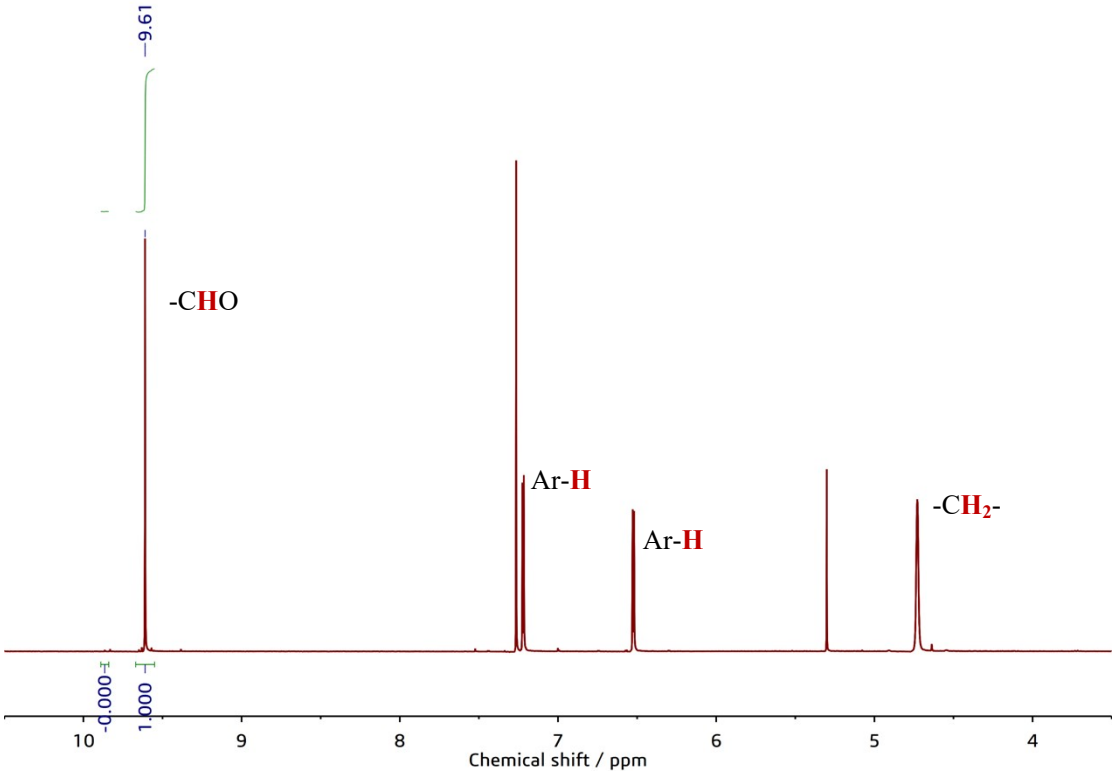

Figure S16. The ^{1}H NMR spectrum of HMF conversion at t=0.

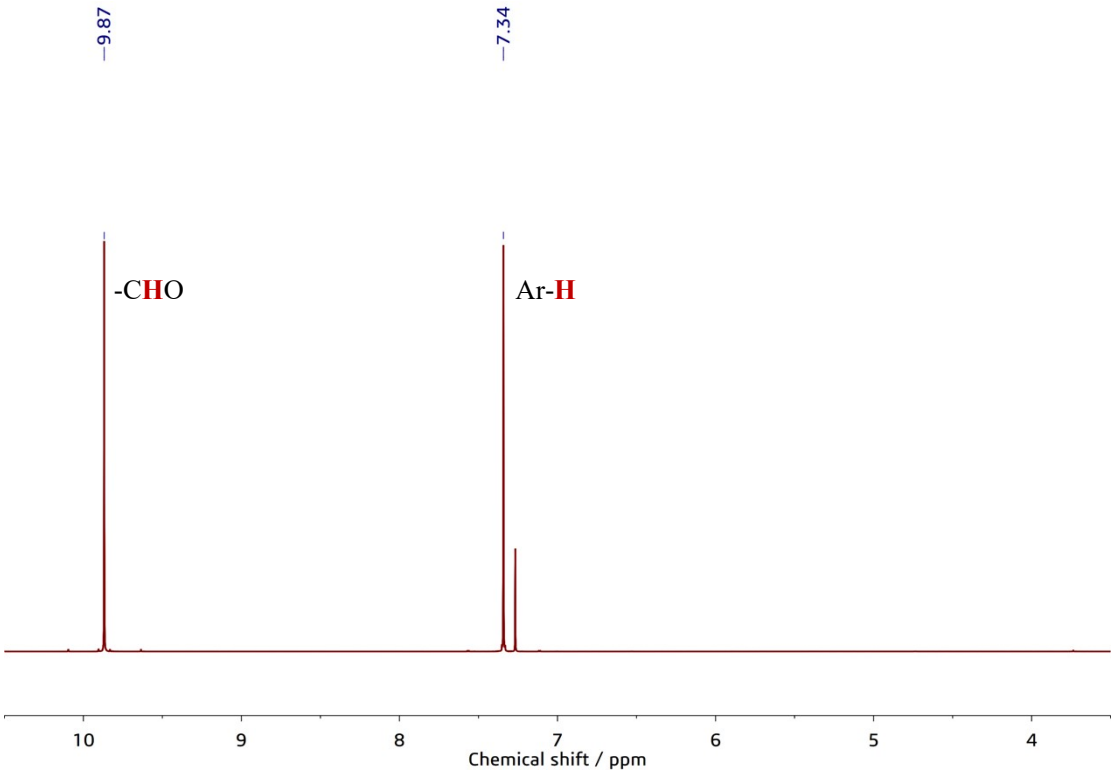

Figure S17. The ^{1}H NMR spectrum of standard DFF in $CDCl_3$.

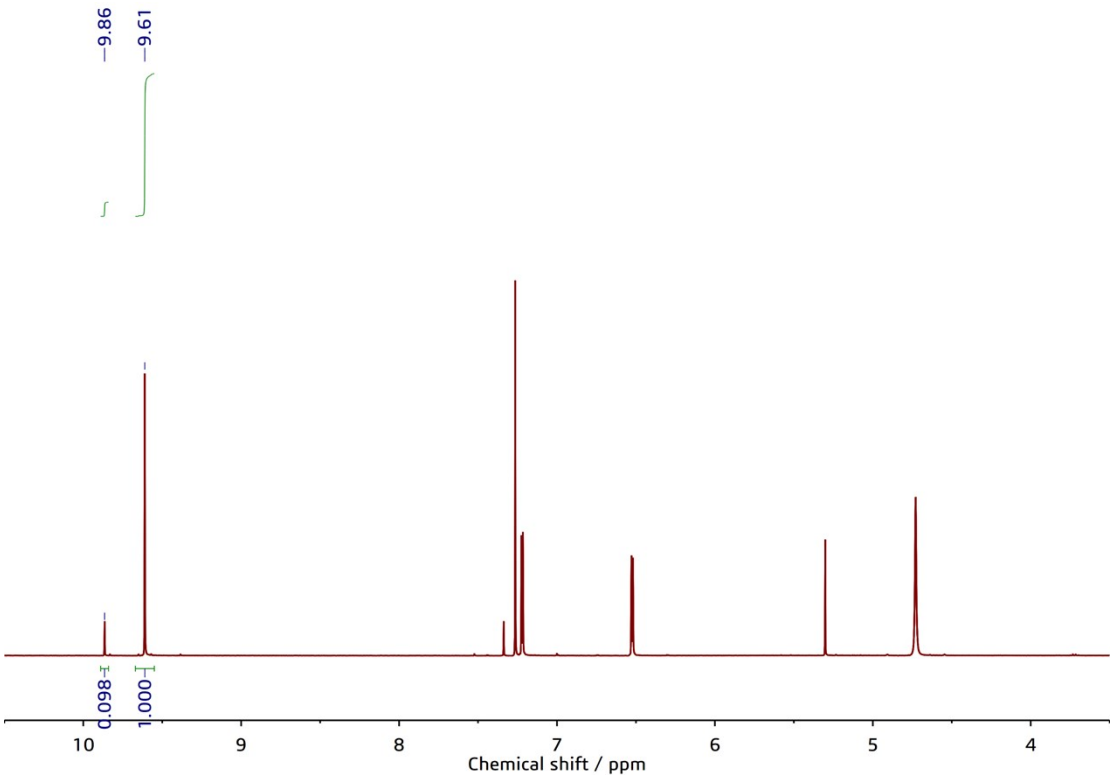

Figure S18. The ^{1}H NMR spectrum of HMF conversion catalyzed by pTBT-En.

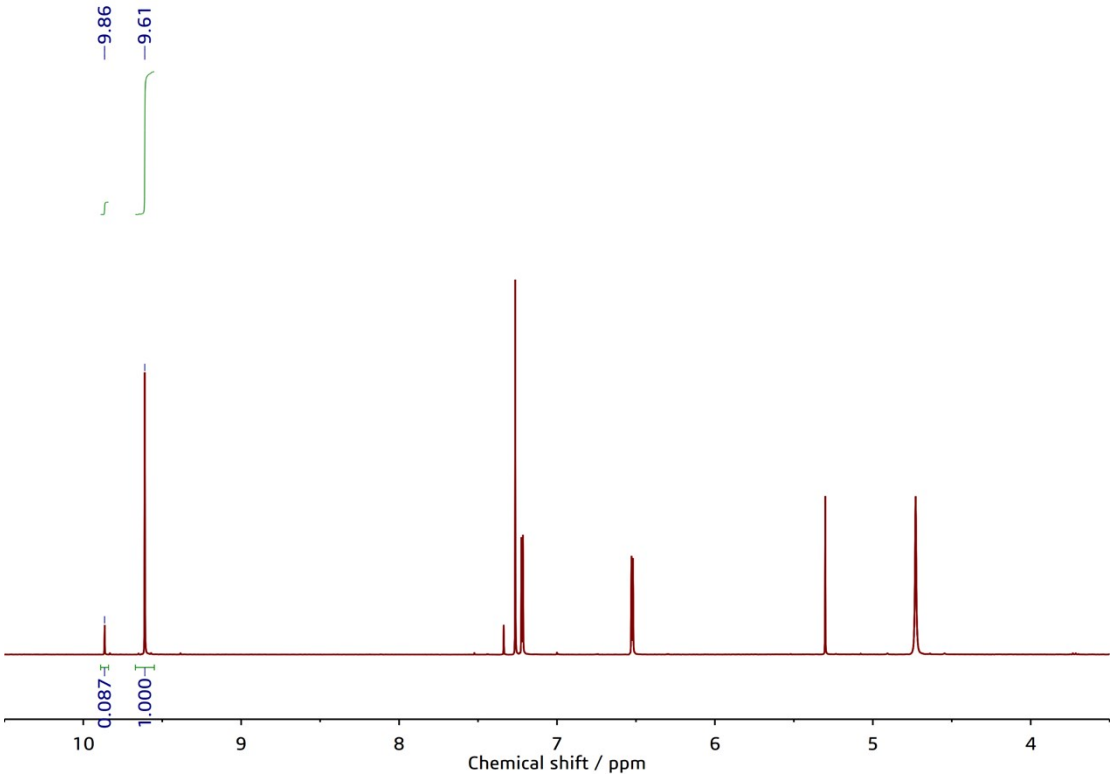

Figure S19. The ^{1}H NMR spectrum of HMF conversion catalyzed by pTBB-En.

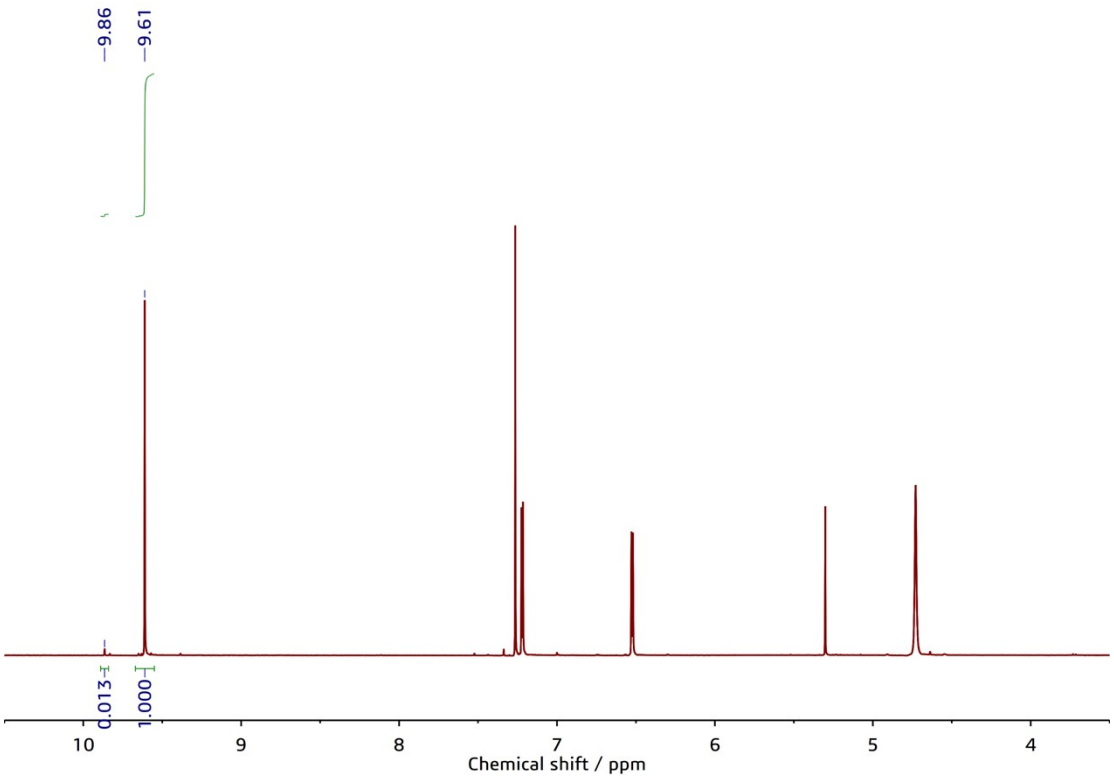

Figure S20. The ^{1}H NMR spectrum of HMF conversion catalyzed by pTBA-En.

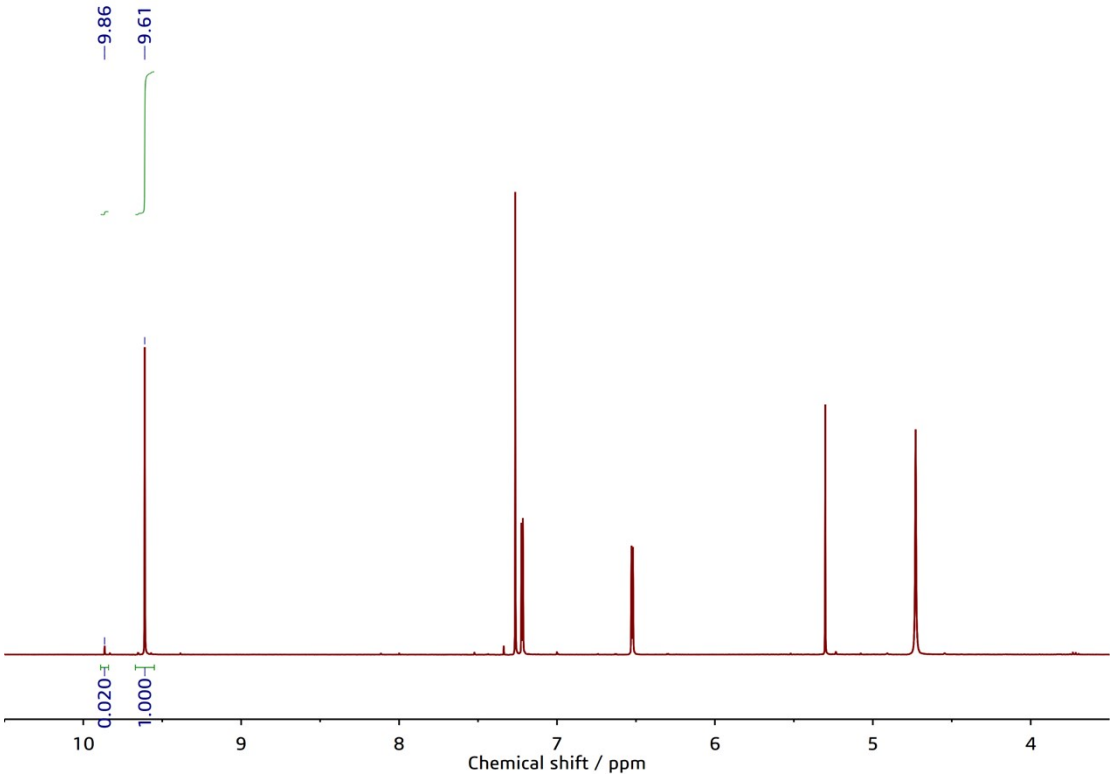

Figure S21. The ^{1}H NMR spectrum of HMF conversion catalyzed by pTBP-En.

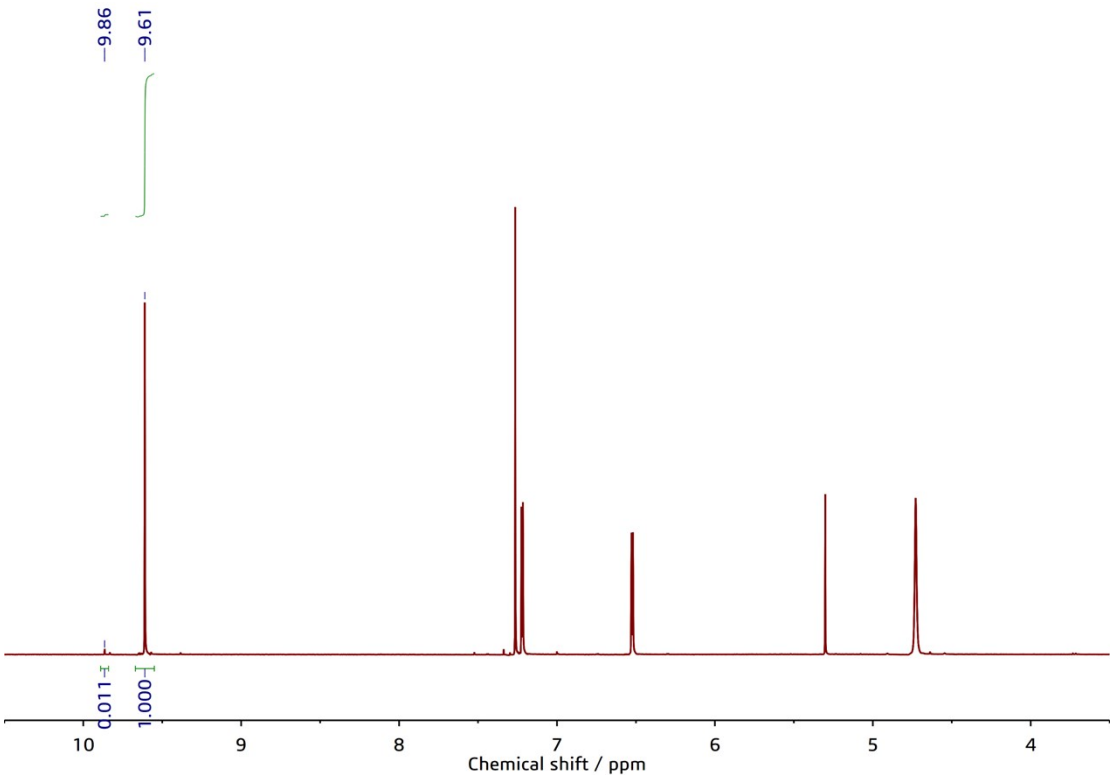

Figure S22. The ^{1}H NMR spectrum of HMF conversion catalyzed by pPYR-En.

Table S6. Photocatalysts for aerobic photocatalytic HMF oxidation.

Photocatalyst	Condition	Product	Production rate
Nb_2O_5 [4]	O_2, 300 W Xe lamp, r.t., benzotrifluoride	DFF	0.29 mmol g^{-1} h^{-1}
g-C_3N_4 [5]	O_2, 300 W Xe lamp, 80°C, H_2O	DFF	0.19 mmol g^{-1} h^{-1}
CTF-Th@SBA-15 [6]	O_2, Xe lamp, r.t., H_2O	DFF	0.19 mmol g^{-1} h^{-1}
pTTT-Ben [7]	air, 40 W 460 nm LED, r.t., H_2O	DFF	0.53 mmol g^{-1} h^{-1}
PHI(Fe) [8]	O_2, 456 nm LED, r.t., H_2O	DFF	0.39 mmol g^{-1} h^{-1}
GZC-2 [9]	O_2, Xe Lamp, r.t., H_2O	DFF	0.40 mmol g^{-1} h^{-1}
pTBT-En (This work)	air, 40 W 460 nm LED, r.t., H_2O	DFF	0.47 mmol g^{-1} h^{-1}
pTBB-En (This work)	air, 40 W 460 nm LED, r.t., H_2O	DFF	0.42 mmol g^{-1} h^{-1}

Table S7. Summary of literature regarding the role of noble metals in photocatalytic reactions.

Photocatalyst	Materials	Application	Noble metal
CP-CMP10 [10]	POPs	Photocatalytic H_2 evolution	Intrinsic Pd
CTF-DCB [11]	CTFs	Photocatalytic H_2 evolution	Extrinsic Pt
COF-JLU35 [12]	COFs	Photocatalytic H_2 evolution	Extrinsic Pt
CTF-BP [13]	CTFs	Photocatalytic H_2O_2 production	Metal free
PD^{2+}-$COF_{16.7}$ [14]	COFs	Photocatalytic H_2O_2 production	Metal free
CTF−Th@SBA-15 [6]	CTFs	Photocatalytic HMF oxidation	Metal free
PANI@CN [15]	g-C_3N_4	Photocatalytic HMF oxidation coupling H_2O_2 production	Metal free

References

1. J. Song, H. Wu, W. Sun, S. Wang, H. Sun, K. Xiao, Y. Qian and C. Liu, *Org. Biomol. Chem.*, 2018, **16**, 2083-2087.
2. X. L. Lv, K. Wang, B. Wang, J. Su, X. Zou, Y. Xie, J. R. Li and H. C. Zhou, *J. Am. Chem. Soc.*, 2017, **139**, 211-217.
3. T. Bura, J. T. Blaskovits and M. Leclerc, *J. Am. Chem. Soc.*, 2016, **138**, 10056-10071.
4. H. Zhang, Q. Wu, C. Guo, Y. Wu and T. Wu, *ACS Sustainable Chem. Eng.*, 2017, **5**, 3517-3523.
5. Q. Wu, Y. He, H. Zhang, Z. Feng, Y. Wu and T. Wu, *Mol. Catal.*, 2017, **436**, 10-18.
6. C. Ayed, W. Huang, G. Kizilsavas, K. Landfester and K. A. I. Zhang, *ChemPhotoChem*, 2020, **4**, 571-576.
7. B. Chen, L. Chen, Z. Yan, J. Kang, S. Chen, Y. Jin, L. Ma, H. Yan and C. Xia, *Green Chem.*, 2021, **23**, 3607-3611.
8. J. B. G. Filho, I. F. Silva, M. Alafandi and J. Rabeah, *Molecules*, 2023, **28**, 8077.
9. M. Guo, T. Zhao, S. Chen, L. Song, B. Xia, J. Ran and S. Z. Qiao, *Adv. Mater.*, 2025, **37**, e10164.
10. R. S. Sprick, J. X. Jiang, B. Bonillo, S. Ren, T. Ratvijitvech, P. Guiglion, M. A. Zwijnenburg, D. J. Adams and A. I. Cooper, *J. Am. Chem. Soc.*, 2015, **137**, 3265-3270.
11. T. Sun, Y. Liang and Y. Xu, *Angew. Chem. Int. Ed.*, 2021, **61**, e202113926.
12. Z. Li, T. Deng, S. Ma, Z. Zhang, G. Wu, J. Wang, Q. Li, H. Xia, S. W. Yang and X. Liu, *J. Am. Chem. Soc.*, 2023, **145**, 8364−8374.
13. L. Zhang, C. Wang, Q. Jiang, P. Lyu and Y. Xu, *J. Am. Chem. Soc.*, 2024, **146**, 29943-29954.
14. F. Hao, C. Yang, X. Lv, F. Chen, S. Wang, G. Zheng and Q. Han, *Angew. Chem. Int. Ed.*, 2023, **62**, e202315456.
15. M. Song, R. Si, J. Han, H. Liu and X. Liao, *Fuel*, 2024, **361**, 130754.